Heliyon 9 (2023) e23101

Contents lists available at ScienceDirect

Heliyon

journal homepage: www.cell.com/heliyon

PVDF/poly(3-methylthiophene)/MWCNT nanocomposites for EMI shielding in the microwave range

Mykhailo V. Petrychuk [a,b,**], Victor V. Oliynyk [b], Volodymyr V. Zagorodnii [b], Nikolay A. Ogurtsov [c], Alexander A. Pud [c,*]

[a] Institute of Biological Information Processing (IBI-3): Bioelectronics, Forschungszentrum Jülich, 52425, Jülich, Germany
[b] Taras Shevchenko National University of Kyiv, Educational Scientific Institute of High Technologies, 01601, Kyiv, Ukraine
[c] V.P. Kukhar Institute of Bioorganic Chemistry and Petro Chemistry of NAS of Ukraine, 50 Kharkivske Shose, Kyiv, 02160, Ukraine

ARTICLE INFO

Keywords:
EMI shielding
Nanocomposites
poly(vinylidene fluoride)
Carbon nanotubes
poly(3-methylthiophene)

ABSTRACT

This work presents a new approach to enhance EMI shielding efficiency of nanocomposites of dielectric polymers, multiwalled carbon nanotubes (MWCNTs) and intrinsically conducting polymers for account of using core-shell morphology for conducting components. To realize this approach new ternary nanocomposites of poly(vinylidene fluoride) (PVDF), MWCNTs and poly(3-methylthiophene) doped by Cl^- anions (P3MT) were prepared through synthesis of thermally stable core/shell nanocomposites PVDF/P3MT and MWCNT/P3MT. These binary nanocomposites were mixed with pure MWCNTs or PVDF followed by compression molding to prepare the ternary nanocomposites of different morphology to discriminate their EMI shielding properties in a wide frequency range (1–67 GHz). Values of the tangent of dielectric loss angle, the efficiency of transmission, reflection and absorption of microwave radiation, and shielding efficiency (SE) of the specified materials were found from analysis of spectral dependences of their complex dielectric constants. It was shown that while the melt mixing of the binary PVDF/P3MT nanocomposite with MWCNTs both in a pure state and in the binary nanocomposite (MWCNT/P3MT) expectedly strongly enhances SE of the former, this effect is non-linear and depends on presence/absence of the P3MT shell on the MWCNT core. The ternary nanocomposite PVDF/P3MT/MWCNT made of the binary polymer-polymer nanocomposite PVDF/P3MT and pure MWCNTs showed highest SE values at the frequencies above 4.5 GHz up to 68.4 dB at 67 GHz in the case of the 1 mm thickness sample. However, below 4.5 GHz the SE was higher in the case of the ternary nanocomposites containing core/shell MWCNT/P3MT nanocomposite instead of pure MWCNT.

1. Introduction

Harmful effects of radiofrequency electromagnetic fields from different electronic devices on our life make a significant pressure on human and other living organisms health and safety, modulate a correct work of these and other devices, etc. [1–5]. These devices are involved in cellular and Internet networks (mobile phones, computers) and even used in recently appeared pain-inflicting military

* Corresponding author.
** Corresponding author. Taras Shevchenko National University of Kyiv, Educational Scientific Institute of High Technologies, 01601, Kyiv, Ukraine.
E-mail addresses: m.petrychuk@gmail.com (M.V. Petrychuk), pud@bpci.kiev.ua (A.A. Pud).

https://doi.org/10.1016/j.heliyon.2023.e23101
Received 17 August 2023; Received in revised form 23 November 2023; Accepted 27 November 2023
Available online 1 December 2023
2405-8440/© 2023 The Author(s). Published by Elsevier Ltd. This is an open access article under the CC BY-NC-ND license (http://creativecommons.org/licenses/by-nc-nd/4.0/).

weapon services. However, while this high-tech electromagnetic emission has a strong negative impact on human life quality, currently no one can stop it because of our needs to use such devices. It seems all we can do in this situation is a development and use of shielding materials suppressing electromagnetic interference (EMI). The shielding materials can be traditionally based on metals or their conducting composites layered complex structures with common polymers, which work as effective screening materials mainly due to a high reflection ability of metals [5,6]. At the same time, such materials are not suitable for many cases because of their high density, corrosion susceptibility, low flexibility, etc. [6,7] and, despite their domination on EMI shielding market, are now replaced in many cases by highly conducting composite materials of polymers filled with magnetic oxides or lightweight carbonaceous particulate matter (carbon black, carbon fibers, carbon nanotubes, graphite, graphene, graphene oxide, etc. [5–11]). Among the carbonaceous materials multiwall carbon nanotubes (MWCNTs) can be considered as one of most suitable fillers due to high conductivity, aspect ratio, specific surface, and a quite acceptable cost [12]. Thus, their combination with metal or ceramic nanoparticles can give nanocomposites, which are good EMI shielding materials [13–16]. In particular, addition of MWCNTs to barium hexaferrite doped with copper, magnesium and zirconium dopants resulted in nanocomposites (mixed with epoxy resin as a binder with the weight percentage of 70:30) having the real and imaginary parts of the permittivity much higher than those of the pure barium hexaferrite based samples. The highly doped sample had a reflection loss (value −23.1 dB at 8 GHz), which was more than twice larger than that of the pure barium hexaferrite based samples in the frequency range 2–18 GHz at a matching thickness of 2.1 mm [13]. The approach involving chemical precipitation of conducting noble metal nanoparticles instead of ceramics on surface of carbonaceous nanomaterials (MWCNTs and reduced graphene oxide (rGO)) and their embedding in a flexible polymer matrix is probably a good choice for formation of lightweight materials with efficient EMI shielding ability [14–16]. In particular, flexible conducting polymer composite films, prepared via a simple solution cast method, of polyvinylidene fluoride (PVDF) loaded with Au nanoparticles −MWCNTs showed effective electromagnetic shielding of 26.7 dB at 12 GHz for 3 wt % Au NPs in 3 wt % MWCNT/PVDF thin (0.5 mm) film [14]. The EMI shielding of 28.5 dB at 12 GHz was observed for the similarly prepared 0.5 mm nanocomposite films of low percentage of metallic nanoparticles (Au, Ag, Cu) decorated MWCNT/rGO reinforcing fillers distributed in the PVDF matrix [15]. Moreover, even better EMI shielding ability was shown for the similarly prepared through the solution cast method 0.1 mm nanocomposite films. In particular, the films with composition of 5 wt% Ag–5 wt% Cu nanoparticles–MWCNT)/PVDF showed a shielding of 26 dB while those of 5 wt% Ag–5 wt.% Cu nanoparticles –rGO/PVDF revealed a shielding of 29 dB in the frequency range of 8–12 GHz [16].

It is known that nature of the non-conducting polymer matrix/binder is of high importance for the reliable and long-term operation of such materials in EMI shielding application [17–19]. To endow these materials necessary properties various polymer binders/matrices were applied such as polyvinyl acetate (PVA), poly(dimethylsiloxane), polyimide, epoxy, PVDF, nylon, polyethylene, polypropylene, ethylene-vinyl acetate copolymers, polystyrene, polyvinylpyrrolidone, sodium alginate, polymethylmethacrylate, etc. [18–22]. Among a variety of common polymers used as the binder PVDF takes a special place due to remarkable set of properties which are characteristic of ferroelectric polymers namely a high permittivity, electroactive properties including ferroelectric, pyroelectric and piezoelectric effects, non-linear optical properties [23]. Its nanocomposites with MWCNT have interesting dielectric properties and high conductivity that allows their applications in EMI shielding, electrostatic dissipation, etc. [14–16,24–29]. For example, 0.3 mm nanocomposite films of PVDF with 4 wt% unfunctionalized of MWCNTs showed the maximum shielding effectiveness values about 110, 45, 30, 26, and 58 dB for L (1–2 GHz), S (2–4 GHz), C (4–5.8 GHz), J (5.8–8 GHz), and X (8–12 GHz) bands, respectively [24]. The solution cast film nanocomposites of Ag/Au decorated MnO_2 nanoparticles and PbS nanocubes embedded Graphene hybrid nanostructures loaded in PVDF matrix revealed significantly higher dielectric constant and electrical conductivity compared to neat PVDF [27,28]. Moreover, the 1 wt% graphene/PbS loaded PVDF thin films nanocomposite displayed good microwave absorption properties the range of 9.5–12 GHz. In the case of the prepared through the same solution route film nanocomposites of mesoporous ZrO_2 and PVDF the EMI SE value was determined to be 7.0 dB at 11 GHz, which is greater than that of a neat PVDF matrix (1.1 dB at 11 GHz) [29].

Importantly that these properties strongly depend on specific interactions between PVDF and carbon nanotubes, which inevitably influence dielectric loss parameters, alignment of MWCNTs in the melt and in turn in the nanocomposite, morphology and as a consequence the shielding efficiency of such materials [30].

EMI shielding and other properties of PVDF based nanocomposites can be also significantly enhanced if, as a third lightweight component, an intrinsically conducting polymer (ICP) is added instead of metal nanoparticles [14–16], metal oxides or PbS nanoparticles components [27–29]. In particular, electromagnetic energy absorption, magnetic, electrical properties and morphology of hybrid nanocomposites of polyvinylidene fluoride (PVDF) with Fe_3O_4 nanoparticles with a shell of polyaniline (PANI) doped by compatibilizing and plasticizing dopant dodecylbenzenesulfonic acid (DBSA) were enhanced compared with the binary nanocomposites without the PANI component [31]. Using MWCNTs with shells of polypyrrole (PPy) doped by dodecylbenzenesulfonate anions as EMI shielding filler in the PVDF matrix allowed to reach for the robust 1 mm PVDF/MWCNT/PPy-DBS nanocomposite film the fairly high values of ~34 dB at 20 GHz [32]. Strong effect of the PPy phase on the properties of such nanocomposites is obviously enhanced by specific interactions of this polymer with carbon nanotubes and with the PVDF phase. Moreover, conductivity, charge state, structure, morphology and other properties of the ICP component can be strongly changed due to intermolecular interactions of ICP with both carbon nanotubes and PVDF as it was shown elsewhere on the example of binary nanocomposites of PPy, polyaniline (PANI) and poly(3-methylthiophene) (P3MT) with MWCNT or PVDF [32–34].

Compared to PPy and PANI composites, poly(3-alkylthiophenes) are rarely mentioned as components of electromagnetic interference shielding materials, while even one of the earliest publications on the matter revealed not bad EMI shielding effectiveness up to ~45 dB for 3 mm thickness films of 20 wt% of poly(3-octylthiophene) blends with polystyrene, polyvinylchloride (PVC) and ethylvinyl acetate (EVA) in the frequency range 100 kHz - 1 GHz [35]. There were a few more attempts to apply composites of polythiophene and its derivatives mainly with ferrites for EMI shielding but with a moderate efficiency less than 25 dB in the range of 1.0–18 GHz [19,36].

However, to our knowledge there are no publications which use technologically suitable and robust ternary polythiophene derivatives nanocomposites with additional carbon nanotubes component embedded in a dielectric polymer matrix for EMI shielding.

This work is devoted to the study of EMI shielding effectiveness of new ternary PVDF/MWCNT/P3MT nanocomposites with application of core-shell morphology for conducting components in a wide frequency range (1–67 GHz) through finding real and imaginary parts of dielectric constant of the nanocomposites with further calculation of the shielding efficiency and its component – reflection, absorption and transmission of electromagnetic radiation.

2. Experimental

2.1. Theoretical background

The interaction of composite materials with electromagnetic radiation (EMR) is characterized by directly measured S-parameters or complex permittivity, which are used to calculate the shielding ability of such materials [37]. In particular, such ability is characterized by the shielding efficiency (SE) [38]:

$$SE[\mathrm{dB}] = 10\log_{10}\frac{P_0}{P_\mathrm{T}}, \tag{1}$$

where P_0 and P_T are the power of the incident and transmitted electromagnetic waves, respectively.

In turn, shielding efficiency in the first approximation consists of the efficiency of reflection (SE_R) and absorption (SE_A).

In this case $SE = SE_\mathrm{R} + SE_\mathrm{A}$. The reflection efficiency is defined as follows:

$$SE_R[\mathrm{dB}] = 10\log_{10}\frac{P_0}{P_0 - P_\mathrm{R}},$$

where P_R is the intensity of reflected electromagnetic waves while the absorption efficiency is defined as:

$$SE_A[\mathrm{dB}] = 10\log_{10}\frac{P_0 - P_\mathrm{R}}{P_\mathrm{T}}.$$

In general, $P_0 = P_\mathrm{R} + P_\mathrm{A} + P_\mathrm{T}$.

At the same time, when calculating the shielding efficiency, more subtle factors of interaction of the electromagnetic wave with the matter are often considered, namely, the presence of a skin layer and multiple reflections and refraction on structural inhomogeneities of mesoscopic sizes [38,39]. The thickness of the skin layer is defined as follows [28]:

$$\delta = \frac{1}{\sqrt{\pi f \mu \sigma}},$$

where $\mu = \mu_0\mu_\mathrm{r}$ – magnetic permeability, σ is specific conductivity of the shielding material.

If we assume that conductivity of non-magnetic nanocomposites is 10^5 S/m, then according to Ref. [40] the thickness of the skin layer at the frequency $f = 10$ GHz is 1 mm. Whereas the specific conductivity of the studied nanocomposites calculated from the measured in this work values of the imaginary part of the permittivity in the frequency range 1–67 GHz, does not exceed 10^3 S/m, the thickness of the skin layer is not less than 10 mm, and, therefore, the effects associated with the skin layer can be ignored in samples with a lower thickness.

The second factor is the multiple reflection and refraction of electromagnetic waves on structural inhomogeneities. It is worth mentioning that the wavelength in vacuum in the applied in this work frequency range 1–67 GHz is not less than ~4.5 mm. Taking into account that the dielectric constant of the samples at the maximum frequency (67 GHz) is not more than 15, the wavelength in the sample is not less than ~ 1 mm. Sizes of inhomogeneities in nanostructured materials are 3–5 orders of magnitude smaller and, therefore, for electromagnetic radiation of the specified frequency the sample material is a homogeneous medium, and interference phenomena at micro-inhomogeneities are practically absent. In this case, for the EMR, the structured medium is continuous with corresponding values of complex dielectric constant. Nevertheless, structural heterogeneities affect the optical characteristics of the material and cause a scattering effect, which is described by the Rayleigh law for the inhomogeneities sizes mentioned above:

$$P_\mathrm{sc} \sim \frac{1}{\lambda^4}, \tag{2}$$

where P_sc is the power of the scattered radiation, λ is wavelength.

Note that expression (2) is derived for dielectric inhomogeneities. Conducting inhomogeneities behavior can differ due to EMR absorption by free charge carriers. This means that in the case of structured nanocomposites, in addition to reflection and absorption the radiation intensity after passing the screen depends also on the scattering conditions on inhomogeneities that, consequently, can increase the efficiency of the EMI absorption. However, an input of the scattering conditions to the total *SE* can be identified and separated through additional study as it requires considerable technical costs. On the other hand, this problem can be bypassed due to the fact that, when measuring the electrodynamic characteristics of the shielding material, the scattering on the inhomogeneities increases the absorption coefficient and, therefore, can be taken into account without considering it as a separate characteristic.

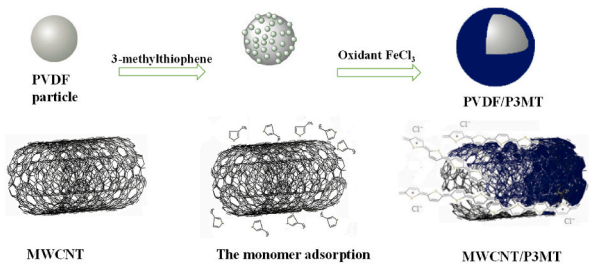

Scheme 1. Formation of binary core/shell PVDF/P3MT and MWCNT/P3MTnanocomposites.

Multiple internal reflections from the interface of the screen and environment affect both the absorption and the reflection coefficient and will be taken into account in the calculations presented hereinafter.

The shielding efficiency *SE*, in accordance with (1), is determined by the ratio of the power of the flux of electromagnetic radiation incident on the test sample to the flux that has passed through the sample. However, the calculated intensity values significantly depend on the thickness of the screen, which influences absorption, scattering and interference of electromagnetic radiation. This suggests that *SE* of shielding materials of different thicknesses can not be correctly compared. Therefore, it is necessary to establish a method for *SE* determination, which allows to correct results for comparison. We propose to use the complex dielectric constant, which determines the characteristics of reflection, absorption and scattering of the EMR. Specifically, taking the known magnitude of the dielectric constant, the values of *SE*, SE_R and SE_A can be determined using Fresnel formulas [41] for a specific screen thickness. Below there are equations expressions to determine the reflection, transmittance, and absorption coefficients for normal incidence, which take into account multiple reflections from the screen surfaces without interference:

$$R = \left(\frac{n^{'}-1}{n^{'}+1}\right)^2, \tag{3}$$

$$T = \frac{4n^{'}}{(n^{'}+1)^2}, \tag{4}$$

$$\alpha = \mathrm{e}^{-2\frac{\omega n^{''} z}{c}}, \tag{5}$$

where $R = \frac{P_R}{P_0}$ and $T = \frac{P_T^{'}}{P_0}$ are the reflectance and transmittance coefficients, respectively, $P_T^{'}$ is the flow that has passed into the medium with $n > 1$, directly behind the interface, $n = n^{'} + jn^{''}$ is the complex refractive index of screening material, $n^{'}$, $n^{''}$ are real and imaginary parts of the complex refractive index (in air $n^{'} = 1$, $n^{''} = 0$), α – absorption coefficient, z is the screen thickness, ω is angular frequency, c is the speed of light in vacuum. Here

$$\begin{aligned} n^{'} &= \sqrt[4]{(\varepsilon^{'})^2 + (\varepsilon^{''})^2} \times \cos\left(\frac{\mathrm{arctg}(\varepsilon^{''}/\varepsilon^{'})}{2}\right) \\ n^{''} &= \sqrt[4]{(\varepsilon^{'})^2 + (\varepsilon^{''})^2} \times \sin\left(\frac{\mathrm{arctg}(\varepsilon^{''}/\varepsilon^{'})}{2}\right) \end{aligned} \tag{6}$$

Taking into account multiple reflections from the interfaces, we obtain the values of the reflection R_∞ and transmittance T_∞ coefficients:

$$R_\infty = R\left(1 + \frac{T^2\alpha^2}{1-\alpha^2R^2}\right), \tag{7}$$

$$T_\infty = \frac{\alpha T^2}{1-\alpha^2R^2}\ . \tag{8}$$

here, T_∞ already determines the part of the flow that has passed through the entire sample, taking into account the multiple reflections from the interfaces. The part of the absorbed energy is equal $A = 1 - R_\infty - T_\infty$.

2.2. Materials and preparations

Acetonitrile (isocratic grade, Merck) was dried before use over annealed 3 Å molecular sieves. Monomer 3-Methylthiophene (3 MT) (Merck), anhydrous $FeCl_3$ (Merck) and other chemicals were of reagent grade and used as received. Submicron powder of 200 nm PVDF particles was prepared by filtration, washing and thorough drying of PVDF Kynar 6000 latex (Arkema). MWCNT (Arkema) were used as received.

Table 1
Description of the formed samples for EMI shielding measurements.

Sample number, #	Composition	Comment
1	Pure PVDF	Reference sample
2	PVDF/P3MT	Made of the binary core/shell PVDF/P3MT nanocomposite
3	PVDF/MWCNT/P3MT	Made of the pure PVDF (90 wt %) and binary core/shell MWCNT/P3MT nanocomposite (10 wt%)
4	PVDF/P3MT/MWCNT	Made of the core/shell nanocomposite PVDF/P3MT (90 wt %) with pure MWCNT (10 wt%)
5	PVDF/P3MT/MWCNT/ P3MT	Made of the core/shell nanocomposite PVDF/P3MT (90 wt %) with the previously synthesized core/shell nanocomposite MWCNT/P3MT (10 wt%)
6	PVDF/P3MT	Second reference sample. Made of the mechanical mixture of pure PVDF and P3MT. Destroyed when treatment to the final cylindrical sample

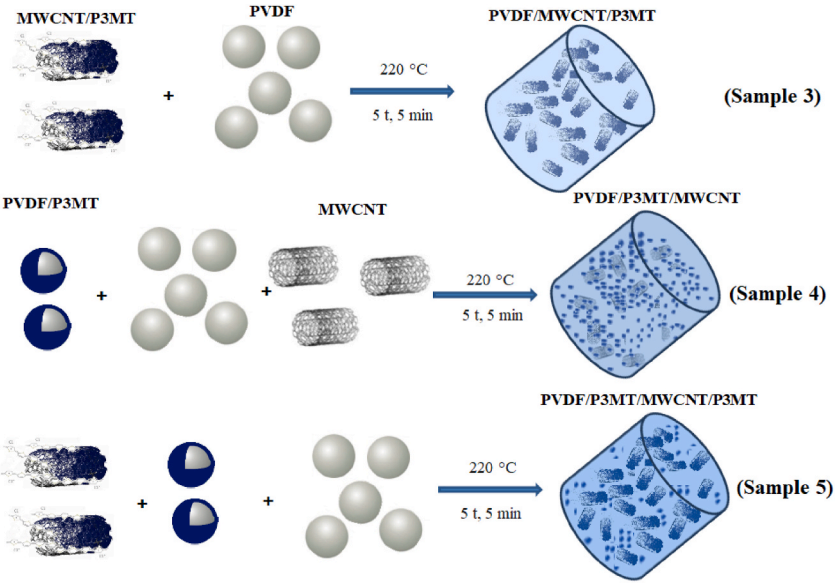

Scheme 2. Illustration of formation of the ternary nanocomposites (samples 3–5, Table 1) fabrication from the binary nanocomposites.

2.3. Preparation of the binary PVDF/P3MT and MWCNT/P3MT core-shell nanocomposites

Based on the synthetic protocol described elsewhere [33], the binary core/shell nanocomposites of PVDF or MWCNTs with P3MT doped by Cl^- anions (abbreviated PVDF/P3MT or MWCNT/P3MT, respectively) were synthesized by chemical oxidative polymerization of 3 MT in thoroughly dried acetonitrile containing dispersed PVDF particles or MWCNTs at a constant temperature of 18 °C (CC1–K6 thermostat, Huber) under stirring and argon atmosphere (Scheme 1).

In the both cases we used the same weight ratio of the dispersed phase (PVDF and MWCNTs) to 3 MT = 90:10. In short, the polymerization was realized as follows. 7.68 g of PVDF or MWCNT powder were dispersed in 60 ml of acetonitrile under ultrasonication for about 20 min and then thermostated at 18 °C. Then 0.854 g of 3 MT (8.7 mmol) was added to this dispersion and stirred for 10 min. The reaction was started by adding 21 ml of the solution of 1.41 g of $FeCl_3$ (8.7 mmol) in acetonitrile and was carried out for 20 h under continuous stirring.

The polymerization mixtures were then centrifuged at 2000 rpm for 20 min to separate the formed nanocomposites. The precipitates were decanted, washed again with acetonitrile and ethanol followed by purification by acetonitrile extraction in a Soxhlet apparatus for 40 h. Completeness of removal of iron salts and other impurities from the nanocomposites was checked by UV–Vis spectra of the mother liquor after the extraction. The purified nanocomposites were finally dried under vacuum at 40 °C to a constant weight. Samples of pure P3MT doped by Cl^- anions (abbreviated here-in-after as P3MT for convenience) were obtained by similar procedures but in the absence of PVDF or MWCNTs.

2.4. Preparation of the binary PVDF/P3MT and ternary PVDF/MWCNT/P3MT melted cylindrical nanocomposites for EMI shielding measurements

The synthesized binary PVDF/P3MT and MWCNT/P3MT nanocomposites were then used to form cylindrical samples (diameter 1.83 mm and height 2.25 mm) for EMI shielding experiments. Previously, the nanocomposite cylinders of larger sizes (diameter 3 mm and height 3 mm) were prepared through thorough mechanical mixing of the binary nanocomposites with pure MWCNT or PVDF in

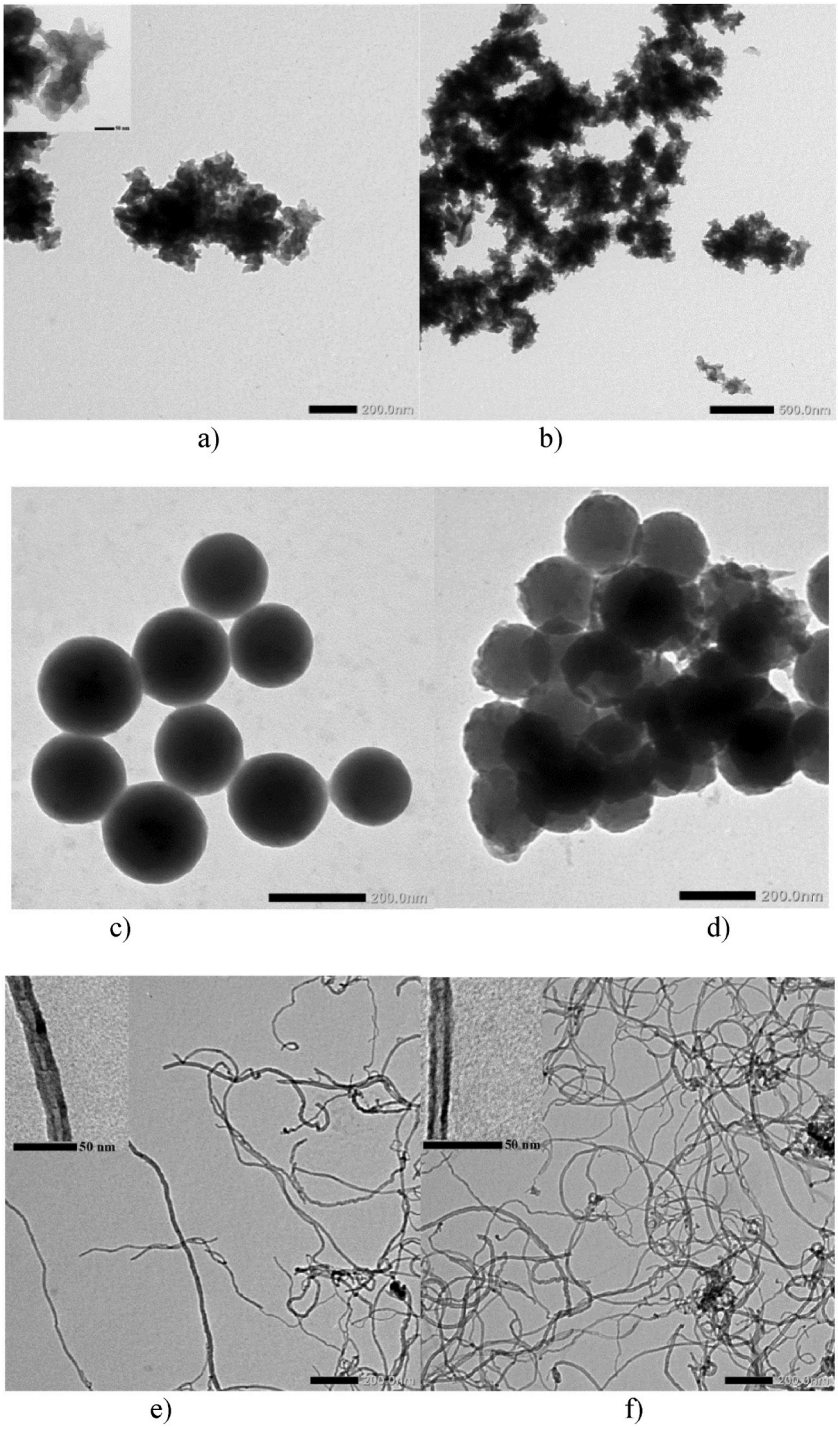

Fig. 1. TEM images of the pure P3MT at different magnifications (a,b), the parent PVDF (c), the core-shell nanocomposite PVDF/P3MT (d), the parent MWCNT (e) and their core-shell nanocomposite MWCNT/P3MT (f). Inserts display TEM images of the materials at the higher magnification.

agate mortar followed by compression molding with the help of Specac press at a load of 5 tons for 5 min at 220 °C (Table 1). These larger cylinders were then treated to get the cylindrical samples with necessary sizes (diameter 1.83 mm and height 2.25 mm).

Schematic presentation of the formation of these ternary nanocomposites (samples 3–5) is shown in Scheme 2.

It is important that the stage of the sample formation showed that a simple mixture of pure PVDF and P3MT (sample 6), even under the long compression molding at the high temperature, did not allow to obtain the mechanically durable material suitable for further testing. At the same time, poor mechanical properties of the sample 6 are the clear evidence of a better compatibility of the synthesized

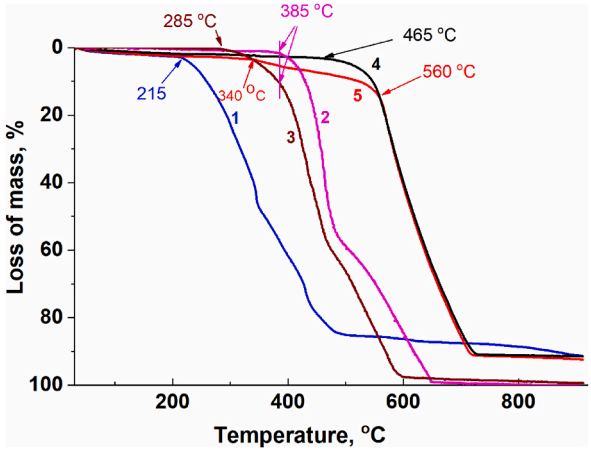

Fig. 2. TG curves of: 1- pure P3MT, 2- parent PVDF, 3- the binary nanocomposite PVDF/P3MT, 4- parent MWCNT and 5- the binary nanocomposite MWCNT/P3MT. 1.5 column.

binary MWCNT/P3MT nanocomposites with the common matrix polymer (PVDF), as well as of the PVDF/P3MT with pure CNTs than in the case of simple mechanical mixture of the pure PVDF and P3MT.

2.5. Characterization

Morphology of the synthesized pure P3MT and these nanocomposites PVDF/P3MT and was visualized by transmission electron microscopy (TEM) with the help of TEM and SEM microscopes JEOL JEM-1400 and JEOL JSM-6060 LV, respectively.

Structural difference between pure P3MT and its phases in the synthesized nanocomposites at the molecular level was estimated by their Fourier transform infrared (FTIR) spectra registered with a resolution of 1 cm^{-1} with the help of Bruker Vertex 70 spectrometer. The spectra were obtained for the samples in KBr pellets.

Thermostability of these nanocomposites was characterized by their thermogravimetry analysis (TGA) in air atmosphere using derivatograph system F. Paulik, J. Paulik, L. Erdey with a heating rate of 10 °C/min.

The main electrodynamic characteristics of the nanocomposites were measured by N5227A PNA Microwave Network Analyzer, (Keysight Technologies) in the wide frequency range from 1 to 67 GHz.

3. Results and discussion

3.1. Morphology and thermal stability of the synthesized binary nanocomposites

3.1.1. TEM

TEM images in Fig. 1 show clear morphological differences between the pure P3MT (a,b) and its phase in the core-shell PVDF/P3MT (c,d) and MWCNT/P3MT (e,f) nanocomposites. In particular, the pure P3MT consists of asymmetric nanoparticles with linear sizes in the range of about 20–70 nm, which are assembled in the large 150–300 nm agglomerates forming in turn the larger aggregates with sizes up to 1 mkm (Fig. 1a and b). However, if P3MT is synthesized in the presence of the spherical sub-micron PVDF particles (~200 nm, Fig. 1c), it forms at their surface inhomogeneous “broken egg”-like shell but almost without agglomeration (Fig. 1d) as it was shown earlier [34]. Most of the P3MT phase is located in these one-two-layered shells in a form of more or less asymmetric nanoparticles like a very poorly shaped spheroids or ellipsoids with sizes in the range of around 10–40 nm. The rest of the P3MT phase forms large agglomerates of the nanoparticles with sizes up to around 50 nm (Fig. 1d).

In the case of the MWCNT/P3MT nanocomposite (Fig. 1f) a state of the P3MT phase is completely different than in the case of the PVDF/P3MT one. There is no separate phase of aggregated P3MT nanoparticles while surface of the carbon nanotubes is inhomogeneously coated with the weakly resolved very thin polymer layer and very small (less than 1 nm) polymer spots.

The morphological differences between the pure P3MT and its counterpart phases in the both nanocomposites are accompanied with peculiarities of their structure, conjugation degree, conductivity and thermostability, etc. Such specificities were recently found for the similar core-shell PVDF/P3MT-Cl nanocomposite with the higher loading of the P3MT phase (the PVDF/3 MT monomer weight ratio 0.6/0.85) [33,35] and for nanocomposites of MWCNTs with other conducting polymers polyaniline [36] and polypyrrole [32]. Here-in-after we will consider the thermostability feature of the synthesized binary nanocomposites which is especially important in terms of their processing at high melting temperatures.

3.1.2. Thermal stability of the synthesized binary nanocomposites

Processing of polymer nanocomposites at high melting temperatures inevitably implies strong demands to their thermal stability, which in turn is predetermined by thermal stability of the composite components and, moreover, can be affected by specific

Table 2
Thermal characteristics of the pure components and synthesized binary nanocomposites.

Sample number, #	Composition	T_5(°C)	T_{30}(°C)	T_{HRI}(°C) or Heat-resistance index/°C
1	pure P3MT	233.9	317.9	139.3
2	pure PVDF	413.3	457.4	210.3
3	PVDF/P3MT	350.8	426.6	194.2
4	pure MWCNT	509.2	583.7	554.4
5	MWCNT/P3MT	372.8	582.1	249.2

$T_{HRI} = 0.49[T_5 + 0.6(T_{30} - T_5)]$, where T_5 and T_{30} are the decomposition temperatures corresponding to 5 % and 30 % weight losses of the samples, respectively [47].

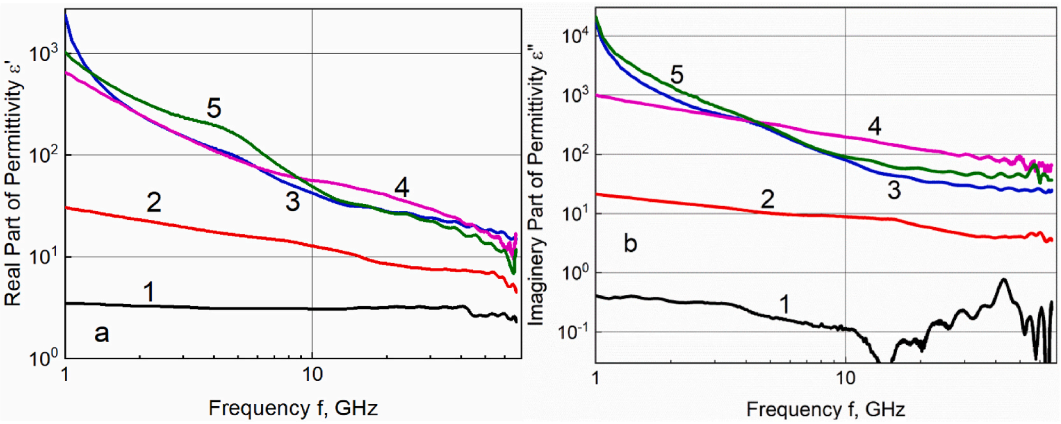

Fig. 3. Frequency dependences of the real (a) and imaginary (b) parts of the complex dielectric permittivity of the samples: 1- PVDF; 2- PVDF/P3MT; 3- PVDF/MWCNT/P3MT; 4– PVDF/P3MT/MWCNT; 5- PVDF/P3MT/MWCNT/P3MT. Relatively small fluctuations of values are a consequence of the residual uncompensated interference arising in the course of the measurements and are not characteristic of the materials under study.

interactions inside the material [32,35,36,42–44]. As one can see from Fig. 2, thermograms of the pristine template materials reveal their high thermal stability. In particular, PVDF is stable up to ~385 °C and shows at higher temperatures typical for this polymer two-step degradation process which includes e.g. elimination of HF, scission and cross-linking of the polymer chains ends [45].

The MWCNTs, after a slight decrease of the weight loss (~1 wt%) typically assigned to the evaporation of water traces, show one-stage degradation above ~ 465 °C. However, the pure P3MT is much less thermally stable. In particular, after the first small weight loss (~1.7 wt%) below 100 °C attributed to the evaporation of adsorbed water [46], the P3MT weight strongly decreases above ~ 215 °C because of elimination of products of thermal oxidative degradation and burning-out of this polymer (Fig. 2).

The situation is dramatically changed in the case of the binary core-shell nanocomposites whose degradation begins at the temperatures intermediate between those of the pure components (Fig. 2). In particular, the shape of their TG traces suggests that the P3MT component is more thermally stable than in the pure state. Indeed, the TG traces of the PVDF/P3MT and MWCNT/P3MT binary nanocomposites are very close with those of the template components up to around 285 °C and 340 °C (Fig. 2), respectively, thus confirming the enhanced stability of the P3MT component in the nanocomposites at high temperatures in air. This enhancement of thermal stability of the P3MT component is supported by the intermediate values of the heat-resistance index (T_{HRI}) of the synthesized binary nanocomposites (PVDF/P3MT and MWCNT/P3MT) and their pure components (Table 2).

This fundamental specificity of such materials is highly important for understanding of changes in properties of the P3MT component which proceed due to its interactions with the template component (PVDF or MWCNT). Existence of such interactions and their influence on the nanocomposite properties was disclosed in detail recently on the example of nanocomposites of PVDF and MWCNTs with different loadings of P3MT [48].

At the same time, from the point of technological preparation of the ternary nanocomposites of PVDF/P3MT/MWCNT at the PVDF high melting treatment temperatures (200–240 °C), the enhanced P3MT-Cl component thermal stability opens a good opportunity for manufacture of these materials for EMI shielding applications.

3.2. The frequency behavior of the complex dielectric permittivity of the nanocomposites

EMI shielding ability of the materials is predetermined by their electromagnetic properties, in particular by the complex dielectric permittivity (ε^*) consisting of real (ε') and imaginary (ε'') parts, respectively reflecting the polarization property of the material and the dissipation/loss of the material, and, moreover, depending on frequency in dispersive materials [49]. Indeed, Fig. 3 confirms changes in the both parts of the permittivity of the nanocomposite samples in the wide frequency range. In particular, the binary polymer-polymer PVDF/P3MT nanocomposite (sample 2) and the ternary nanocomposites with MWCNTs (samples 3–5) show a

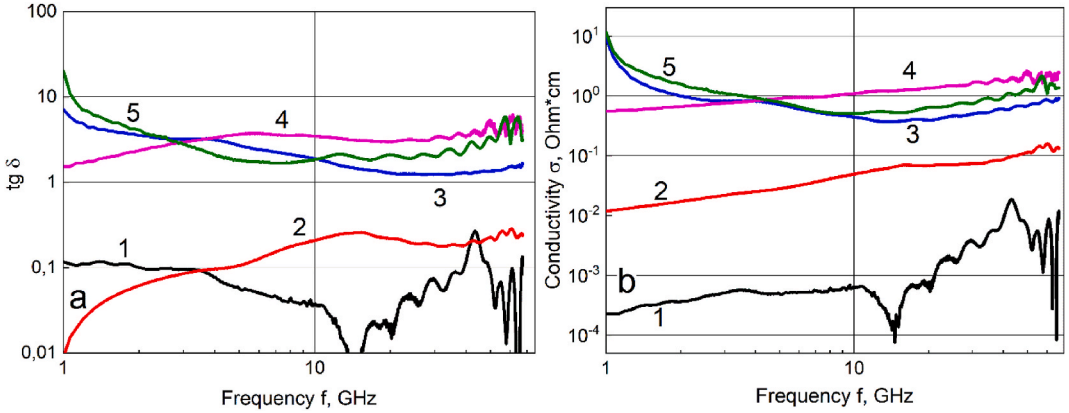

Fig. 4. Frequency dependences of the effective loss tangent (a) and corresponding conductivity (b) for the samples: 1- PVDF; 2- PVDF/P3MT; 3- PVDF/MWCNT/P3MT; 4– PVDF/P3MT/MWCNT; 5- PVDF/P3MT/MWCNT/P3MT.

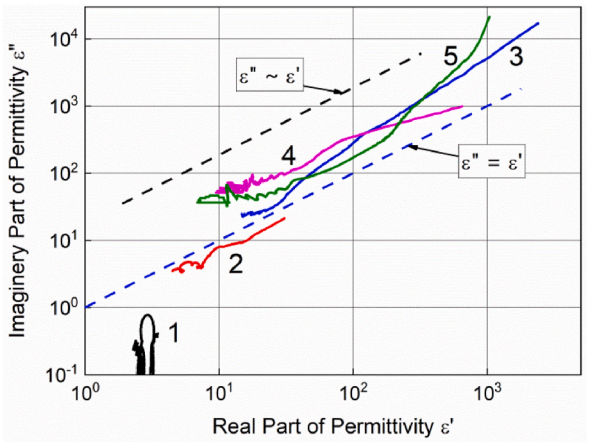

Fig. 5. Dependences $\varepsilon''(\varepsilon')$ (Cole-Cole diagrams) for the samples: 1- PVDF; 2- PVDF/P3MT; 3- PVDF/MWCNT/P3MT; 4- PVDF/P3MT/MWCNT; 5- PVDF/P3MT/MWCNT/P3MT.

significant dispersion of the both parts in the whole frequency range 1–67 GHz (Fig. 3a and b) which is caused obviously by interfacial polarization, orientation and electronic polarization typical of the composite materials [49]. These phenomena lead to significant variations in reflection and absorption of these samples at different frequencies. In turn, this suggests that the P3MT nanoparticles localized in the shell of the binary core-shell PVDF/P3MT nanocomposite (Fig. 1d), after its melting and formation of the monolithic nanocomposite PVDF/P3MT (sample 2), are dispersed inside the sample and form a conducting percolation network.

As one can see, in the case of the polymer samples 1 (pure PVDF) and 2 (the binary PVDF/P3MT nanocomposite) the real part ε' exceeds the imaginary one ε'' in the whole frequency range. However, the behavior of the ternary nanocomposite samples 3–5 (with additional conducting MWCNTs component) is opposite i.e. the magnitude of ε'' prevails. In the latter case this suggests that the samples 3–5 have higher losses due to their conductivity. The losses are well illustrated by the frequency dependences of the effective loss tangent (the ratio of the imaginary part to the real part of the complex permittivity) $\tan\delta = \varepsilon''/\varepsilon'$ especially for the nanocomposites with MWCNTs with the P3MT shell (only samples 3 and 5, Table 1) (see Fig. 4a). Fig. 4b shows the conductivity spectra of the samples calculated by the formula:

$$\sigma = \frac{\varepsilon''}{4\pi}\omega, \tag{12}$$

where ω is the angular frequency.

We see that the conductivity of samples 3 and 5 increases with decreasing frequencies in the $f < 10$ GHz range, which is characteristic of Maxwell-Wagner polarization, i.e. in this frequency range the charges still have time to move through the cluster. At higher frequencies, and in samples 1, 2 and 4 in the entire frequency range, the conductivity seems to be determined by other mechanisms.

In fact, the $\tan\delta$ behavior (Fig. 4a) shows the specificity of these ternary samples with the P3MT component tightly bound to the surface of MWCNTs as compared with the samples 2 and 4 containing the separate phase of P3MT nanoparticles (stemmed from the

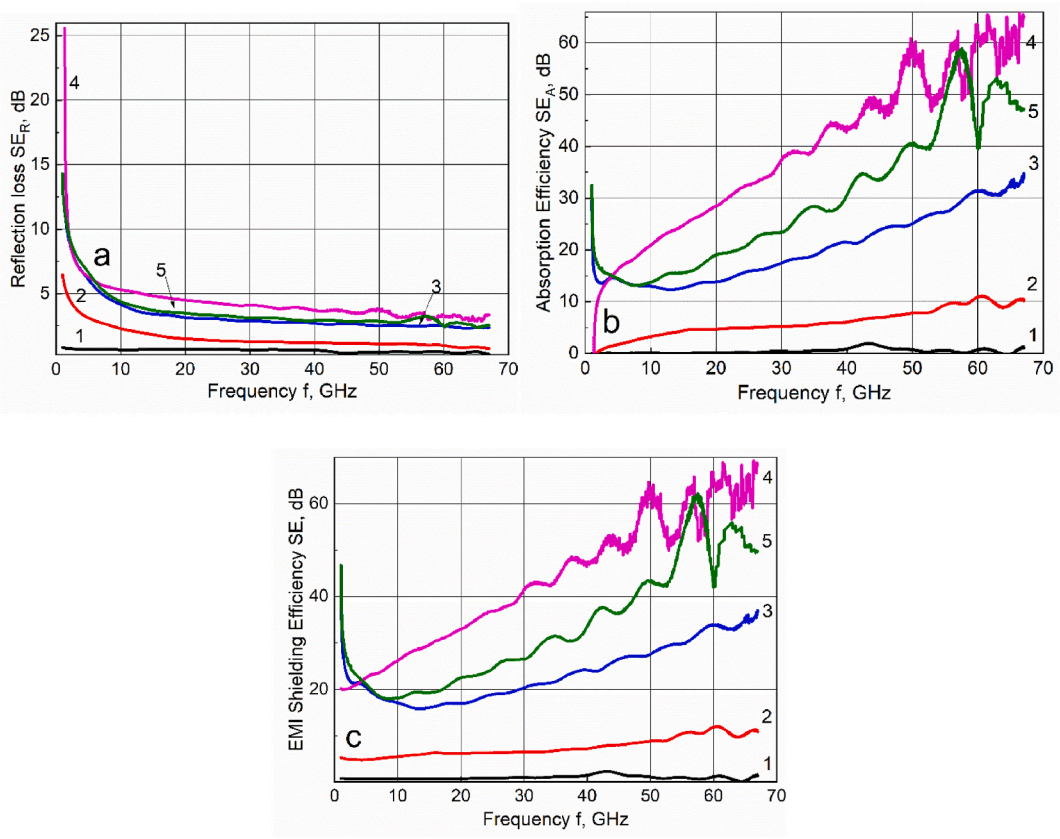

Fig. 6. Dependences of reflection loss SE_R (a), absorption efficiency SE_A (b), and EMI shielding efficiency SE (c) on the frequency for the samples: 1-PVDF; 2- PVDF/P3MT; 3- PVDF/MWCNT/P3MT; 4– PVDF/P3MT/MWCNT; 5- PVDF/P3MT/MWCNT/P3MT.

parent PVDF/P3MT, see TEM image Fig. 1d and Table 1). In particular, this behavior not only reveals the fact that the former materials have the increased losses at the beginning (f = 1–4 GHz) of the whole frequency range followed by the lowered losses at higher frequencies (as compared with the latter materials) but also confirms the above-discussed specific interactions and properties of the P3MT with MWCNTs formed in the binary MWCNT/P3MT nanocomposite.

At the same time, the real and imaginary parts of the complex permittivity in the samples 3 and 4 with coated and uncoated nanotubes practically coincide in the quite narrow frequency ranges about 1.5 GHz–6 GHz and 2.6 GHz–4.5 GHz (Fig. 4), respectively. In the samples 3 and 5 differing in the latter case by the presence of the P3MT nanoparticles (separate phase) from the shells of PVDF/P3MT (Table 1), the real and imaginary parts of the complex permittivity coincide also in the ranges 12 GHz–30 GHz and 4 GHz–10 GHz, respectively. For the moment there is no clear understanding why we observe this phenomenon and further deeper investigations of the physical-chemical interactions and state of these materials are needed. Nevertheless, existence of this phenomenon can be partially explained by the presence of some factor(s) compensating the difference between the materials in these frequency ranges.

Fig. 5 shows the $\varepsilon''(\varepsilon')$ dependences. Only for the sample 1 (pure PVDF) there is a curve that remotely resembles the curve for an oscillator with one time constant. For other samples, the dependences close to the linear one $\varepsilon'' \sim \varepsilon$ are observed. The sample 5 shows almost quadratic dependence at high frequencies.

3.3. EMI shielding effectiveness of the ternary nanocomposites

SE, SE_R and SE_A parameters, calculated in accord with equations (3)–(8) for the nanocomposites 2–5, are presented in Fig. 6 on the example of the samples with the thicknesses reduced to 1 mm, for convenience. Expectedly the binary polymer-polymer nanocomposite 2 shows the much lower reflection, absorption and shielding properties than the ternary ones with carbon nanotubes. Nevertheless, there is a general trend to monotonous decreasing the reflection loss with the frequency growth from 6 to 10 dB at ~2 GHz to ~ 1–3 dB at 67 GHz. As a result, the main contribution to the shielding efficiency (SE) of the samples is made by absorption, and this trend strongly increases above ~1.8 GHz when SE_R becomes lower 10 dB with increasing frequency (Fig. 6a–c).

At the same time, there is a significant difference in the behavior between the nanocomposite samples containing separate P3MT nanoparticles dispersed inside the PVDF matrix (samples 2 and 4) and the nanocomposite samples with P3MT component tightly bound to the surface of MWCNTs (samples 3 and 5) (Fig. 6b and c). Thus, the former show a quite strong monotonous growth of SE_A

Table 3
Comparison of SE values for the binary polymer-polymer nanocomposite (sample 2) and ternary nanocomposites containing binary MWCNT/P3MT nanocomposite pure or MWCNTs (sample 4) (samples 3, 5) at fixed frequencies.

GHz SE	Frequency, GHz			
	1	2	15	67
PVDF/P3MT (sample 2)	**5.3**	**5.0**	**6.2**	**10.9**
PVDF/MWCNT/P3MT (sample 3)	**43.7**	**26.5**	**16.1**	**37.1**
PVDF/P3MT/MWCNT (sample 4)	**20.2**	**20.1**	**29.6**	**68.4**
PVDF/P3MT/MWCNT/P3MT (sample 5)	**46.8**	**23.8**	**19.3**	**50.0**

and SE (Fig. 6b and c). The pure (untreated) MWCNTs in the nanocomposite (sample 4) increase almost linearly the SE and SE_A values in 5–7 times in the whole frequency range as compared with the binary nanocomposite (sample 2). This almost linear change in the protection capability when transition from sample 2 to sample 4 reveals a more significant input of the MWCNTs in their shielding efficiency as compared with the P3MT component. The situation is strongly different in the case of the nanocomposites with the MWCNTs coated with the P3MT (samples 3 and 5) which demonstrate, in particular, decreasing SE from ~44 dB (sample3) and ~46 dB (sample 5) at 1 GHz to a common wide minimum around 18 dB followed by increasing to ~37 dB (sample 3) and ~50 dB (sample 5) (Fig. 6c). This behavior of the both samples (3 and 5) in the whole frequency range suggests a specific state of the P3MT component localized in the shells on the MWCNTs which can lead to lowering its absorption ability in the low frequency range (1–10 GHz). This trend is, however, reversed at higher frequencies probably due to the absorption ability of MWCNT component (Fig. 6c). Nevertheless, one can see the higher shielding efficiency in the ranges around 1–4.2 GHz and 7.8–67 GHz in the case of sample 5 due to probably, the absorption of the separate P3MT nanoparticles in addition to core-shell MWCNT/P3MT binary nanocomposites. This effect can not be considered as an additive input of the former component because differences between SE values of the both samples (5 and 3) at fixed frequencies differ from with SE values of the sample 2 in these frequency ranges (Table 3).

At the same time, non-additivity of SE inputs of two binary nanocomposites (PVDF/P3MT and MWCNT/P3MT) confirms an existence of specific interactions in the final ternary nanocomposite (sample 5) between separate P3MT nanoparticles, formed for the former one, and P3MT shells at the MWCNTs cores.

4. Conclusions

New ternary nanocomposites of poly(vinylidene fluoride) (PVDF) multiwalled carbon nanotubes (MWCNT) and poly(3-methylthiophene) (P3MT) have been prepared for EMI shielding. Specificity of these nanocomposites consists in the fact that they are made by compression molding of mixtures of bare PVDF or MWCNTs with previously synthesized binary nanocomposites PVDF/P3MT and/or MWCNT/P3MT of core/shell morphology. This approach allowed preparing the ternary nanocomposites of different morphology to discriminate their EMI shielding properties in a wide frequency range from 1 GHz up to 67 GHz. In particular, using core/shell PVDF/P3MT nanocomposite for such preparation leads to appearance of P3MT nanoparticles from the P3MT shell in the ternary nanocomposite bulk. These nanoparticles form own conducting percolation network in addition to pure MWCNTs or MWCNT/P3MT percolation networks and affect spectral dependences of complex dielectric constants of ternary nanocomposites and finally EMI shielding efficiency. In particular, in the case of nanocomposites made of the binary polymer-polymer nanocomposite PVDF/P3MT and of its mixture with pure MWCNTs almost a monotonous growth of absorption and shielding efficiency (SE_A and SE) in the wide frequency ranges is observed. However, if the ternary nanocomposites contained the binary core/shell nanocomposite MWCNT/P3MT, some decrease of these efficiencies was observed in the range of 1–9.5 GHz followed then by their mild growth up to 67 GHz. As a result, the best SE_A and SE values above 4.5 GHz were shown by the ternary nanocomposite containing both P3MT nanoparticles and pure MWCNTs while at lower frequencies SE_A and SE values were higher in the case of the ternary nanocomposites containing core/shell MWCNT/P3MT nanocomposite instead of pure MWCNTs. This non-additivity of the inputs of two binary nanocomposites (PVDF/P3MT and MWCNT/P3MT) confirms an existence of specific interactions in the final ternary nanocomposite between separate P3MT nanoparticles, formed for the former one, and P3MT shells at the MWCNTs cores.

It is worth noting that the developed nanocomposites are characterized by an increase of the contributions of absorption and a decrease of the reflection toward total SE with increasing frequency, which appear positive for using these materials for EMI shielding of electronic equipment and as protective coatings reducing radio visibility.

Data availability statement

Data will be made available on request.

CRediT authorship contribution statement

Mykhailo V. Petrychuk: Writing - original draft, Validation, Formal analysis, Data curation, Conceptualization. **Victor V. Oliynyk:** Resources, Methodology, Investigation. **Volodymyr V. Zagorodnii:** Resources, Methodology, Investigation, Data curation. **Nikolay A. Ogurtsov:** Resources, Methodology, Investigation, Formal analysis. **Alexander A. Pud:** Writing - review & editing, Writing - original draft, Supervision, Project administration, Conceptualization.

Declaration of competing interest

The authors declare that they have no known competing financial interests or personal relationships that could have appeared to influence the work reported in this paper.

Acknowledgments

The authors are grateful to Dr. Dmytro Sydorov for assistance with the samples preparation.

References

[1] Non-ionizing Radiation, Part II: Radiofrequency Electromagnetic Fields, IARC Working Group on the Evaluation of Carcinogenic Risks to Humans, Lyon, France, 2011. https://monographs.iarc.who.int/wp-content/uploads/2018/06/mono102.pdf.
[2] A. Thielens, D. Bell, D.B. Mortimore, M.K. Greco, L. Martens, W. Joseph, Exposure of insects to radio-frequency electromagnetic fields from 2 to 120 GHz, Sci. Rep. 8 (2018) 3924, https://doi.org/10.1038/s41598-018-22271-3.
[3] A. Schoeni, K. Roser, M. Röösli, Memory performance, wireless communication and exposure to radiofrequency electromagnetic fields: a prospective cohort study in adolescents, Environ. Int. 85 (2015) 343–351, https://doi.org/10.1016/j.envint.2015.09.025.
[4] WHO Fact sheet N°226 Electromagnetic fields and public health: radars and human health, https://www.who.int/peh-emf/publications/facts/fs226/en/.
[5] S. Sankaran, K. Deshmukh, M.B. Ahamed, S.K.K. Pasha, Recent advances in electromagnetic interference shielding properties of metal and carbon filler reinforced flexible polymer composites: a review, Composites Part A 114 (2018) 49–71, https://doi.org/10.1016/j.compositesa.2018.08.006.
[6] B. Zhao, C. Zhao, R. Li, S.M. Hamidinejad, C.B. Park, Flexible, ultrathin, and high-efficiency electromagnetic shielding properties of poly(vinylidene fluoride)/carbon composite films, ACS Appl. Mater. Interfaces 9 (2017) 20873–20884, https://doi.org/10.1021/acsami.7b04935.
[7] H. Nallabothula, Y. Bhattacharjee, L. Samantara, S. Bose, Processing-mediated different states of dispersion of multiwalled carbon nanotubes in PDMS nanocomposites influence EMI shielding performance, ACS Omega 4 (2019) 1781–1790, https://doi.org/10.1021/acsomega.8b02920.
[8] Z. Zeng Z, H. Jin, M. Chen, W. Li, L. Zhou, Z. Zhang, Lightweight and anisotropic porous MWCNT/WPU composites for ultrahigh performance electromagnetic interference shielding, Adv. Funct. Mater. 26 (2016) 303–310, https://doi.org/10.1002/adfm.201503579.
[9] Y. Wang, T. Li, L. Zhao, Z. Hu, Y. Gu, Research progress on nanostructured radar absorbing materials, Energy Power Eng. 3 (2011) 580, https://doi.org/10.4236/epe.2011.34072.
[10] K. Sabira, M.P. Jayakrishnan, P. Saheeda, S. Jayalekshmi, On the absorption dominated EMI shielding effects in free standing and flexible films of poly (vinylidene fluoride)/graphene nanocomposite, Eur. Polym. J. 99 (2018) 437–444, https://doi.org/10.1016/j.eurpolymj.2017.12.034.
[11] A. Katheria, P. Das, J. Nayak, K. Nath, S.K. Ghosh, S. Paul, N.C. Das, Tailored distribution of 1D nanoparticles in co-continuous EMA/TPO flexible polymeric blends used as emerging materials for suppressing electromagnetic radiation, J. Phys. Chem. Solid. 179 (2023), 111395, https://doi.org/10.1016/j.jpcs.2023.111395.
[12] R. Rao, C.L. Pint, A.E. Islam, R.S. Weatherup, S. Hofmann, E.R. Meshot, F. Wu, C. Zhou, N. Dee, et al., Carbon nanotubes and related nanomaterials: critical advances and challenges for synthesis toward mainstream commercial applications, ACS Nano 12 (2018) 11756–11784. https://pubs.acs.org/doi/10.1021/acsnano.8b06511.
[13] H. Nikmanesh, M. Moradi, G.H. Bordbar, R.S. Alam, Synthesis of multi-walled carbon nanotube/doped barium hexaferrite nanocomposites: an investigation of structural, magnetic and microwave absorption properties, Ceram. Int. 42 (2016) 14342–14349, https://doi.org/10.1016/j.ceramint.2016.05.089.
[14] R. Kumaran, S. Dinesh Kumar, N. Balasubramanian, M. Alagar, V. Subramanian, K. Dinakaran, Enhanced electromagnetic interference shielding in an Au-MWCNT composite nanostructure dispersed PVDF thin films, J. Phys. Chem. C 120 (2016) 13771–13778, https://doi.org/10.1021/acs.jpcc.6b01333.
[15] R. Kumaran, S. Dinesh Kumar, M. Alagar, B. Natesan, V. Subramanian, K. Dinakaran, Electromagnetic interference (EMI) shielding performance of lightweight metal decorated carbon nanostructures dispersed in flexible polyvinylidene fluoride films, New J. Chem. 42 (2018) 12945–12953, https://doi.org/10.1039/C8NJ02460J.
[16] R. Kumaran, A. Vinaya Kumar, M. Alagar, S. Dinesh Kumar, V. Subramanian, K. Dinakaran, Enhanced shielding of electromagnetic radiations with flexible, light-weight, and conductive Ag-Cu/MWCNT/rGO architected PVDF nanocomposite films, Polym. Adv. Technol. 32 (2021) 3759–3769, https://doi.org/10.1002/pat.5395.
[17] Y. Bhattacharjee, I. Arief, S. Bose, Recent trends in multilayered architectures towards screening electromagnetic radiation: challenges and perspectives, J. Mater. Chem. C 5 (2017) 7390–7403. https://pubs.rsc.org/en/content/articlelanding/2017/tc/c7tc02172k.
[18] D. Jiang, V. Murugadoss, Y. Wang, J. Lin, T. Ding, Z. Wang, Q. Shao, C. Wang, H. Liu, N. Lu, R. Wei, A. Subramania, Z. Guo, Electromagnetic interference shielding polymers and nanocomposites - a review, Polym. Rev. 59 (2019) 280–337, https://doi.org/10.1080/15583724.2018.1546737.
[19] S. Ganguly, P. Bhawal, R. Ravindren, N.C. Das, Polymer nanocomposites for electromagnetic interference shielding: a review, J. Nanosci. Nanotechnol. 18 (2018) 7641–7669, https://doi.org/10.1166/jnn.2018.15828.
[20] X. Tan, Q. Yuan, M. Qiu, J. Yu, N. Jiang, C.-T. Lin, W. Dai, Rational design of graphene/polymer composites with excellent electromagnetic interference shielding effectiveness and high thermal conductivity: a mini review, J. Mater. Sci. Technol. 117 (2022) 238–250, https://doi.org/10.1016/j.jmst.2021.10.052.
[21] R.B. Jagadeesh Chandra, B. Shivamurthy, S.D. Kulkarni, M.S. Kumar, Mater. Res. Express 6 (2019), 082008, https://doi.org/10.1088/2053-1591/aaff00.
[22] N. Kavitha, A. Chandramohan, D. Sharma, K. Dinakaran, Synthesis and microwave absorption studies on 2D graphitic carbon nitride loaded polyaniline/polyvinyl alcohol nanocomposites, High Perform. Polym. 35 (2023) 324–337, https://doi.org/10.1177/09540083221134955.
[23] C. Ribeiro, C.M. Costa, D.M. Correia, J. Nunes-Pereira, J. Oliveira, P. Martins, R. Gonçalves, V.F. Cardoso, S. Lanceros-Méndez, Electroactive poly(vinylidene fluoride)-based structures for advanced applications, Nat. Protoc. 13 (2018) 681–704. https://www.nature.com/articles/nprot.2017.157.
[24] G.S. Kumar, D. Vishnupriya, A. Joshi, S. Datar, T.U. Patro, Electromagnetic interference shielding in 1–18 GHz frequency and electrical property correlations in poly (vinylidene fluoride) – multi-walled carbon nanotube composites, Phys. Chem. Chem. Phys. 17 (2015) 20347–20360, https://doi.org/10.1039/C5CP02585K.
[25] R. Simoes, J. Silva, R. Vaia, V. Sencadas, P. Costa, J. Gomes, S. Lanceros-Méndez, Low percolation transitions in carbon nanotube networks dispersed in a polymer matrix: dielectric properties, simulations and experiments, Nanotechnology 20 (2009), 035703, https://doi.org/10.1088/0957-4484/20/3/035703.
[26] J. Banerjee, D. Kingshuk, Melt-mixed carbon nanotubes/polymer nanocomposites, Polym. Compos. 40 (2019) 4473–4488, https://doi.org/10.1002/pc.25334.
[27] K. Narayanasamy, S.S. Sekar, R. Rajakumari, R. Suresh Kumar, D. Roy, K. Dinakaran, Synthesis and characterization of Ag/Au-MnO2 nanostructure embedded polyvinylidine difluoride high K nanocomposites, Int. J. Polym. Anal. Char. 26 (2021) 37–46, https://doi.org/10.1080/1023666X.2020.1840864.
[28] K. Dinakaran, K. Narayanasamy, S. Theerthagiri, P. Peethambaram, S. Krishnan, D. Roy, Microwave absorption and dielectric behavior of lead sulfide – graphene composite nanostructure embedded polyvinylidinedilfuoride thin films, Int. J. Polym. Anal. Char. 27 (2022) 277–288, https://doi.org/10.1080/1023666X.2022.2067958.
[29] T. Gayathri, N. Kavitha, A. Chandramohan, D. Roy, K. Dinakaran, Mesoporous zirconia nanostructures embedded Polyvinyledine difluoride conducting films for EMI shielding applications, Mater. Today: Proc. 59 (2022) 534–539, https://doi.org/10.1016/j.matpr.2021.11.564.
[30] A. Gebrekrstos, S. Biswas, A.V. Menon, G. Madras, P. Pötschke, S. Bose, Multi-layered stack consisting of PVDF nanocomposites with flow-induced oriented MWCNT structure can supress electromagnetic radiation, Composites, Part B 166 (2019) 749–757, https://doi.org/10.1016/j.compositesb.2019.03.008.
[31] M. Petrychuk, V. Kovalenko, A. Pud, N. Ogurtsov, A. Gubin, Ternary magnetic nanocomposites based on core–shell Fe3O4/polyaniline nanoparticles distributed in PVDF matrix, Phys. Status Solidi A 207 (2009) 442–447, https://doi.org/10.1002/pssa.200824421.

[32] A. Ogurtsov, YuV. Noskov, O.S. Kruglyak, S.I. Bohvan, V.V. Klepko, M.V. Petrichuk, A.A. Pud, Effect of the dopant anion and oxidant on the structure and properties of nanocomposites of polypyrrole and carbon nanotubes, Theor. Exp. Chem. 54 (2018) 114–121, https://doi.org/10.1007/s11237-018-9554-x.
[33] N.A. Ogurtsov, V.N. Bliznyuk, A.V. Mamykin, O.L. Kukla, YuP. Piryatinski, A.A. Pud, Poly (vinylidene fluoride)/poly (3-methylthiophene) core–shell nanocomposites with improved structural and electronic properties of the conducting polymer component, Phys. Chem. Chem. Phys. 20 (2018) 6450–6461, https://doi.org/10.1039/C7CP07604E.
[34] V. Bliznyuk, A. Pud, L. Scipioni, C. Huynh, N. Ogurtsov, D. Ferranti, Structure and properties of polymer core-shell systems: helium ion microscopy and electrical conductivity studies, J. Vac. Sci. Technol., B 28 (2010) C6P59–C6P65, https://doi.org/10.1116/1.3504589.
[35] A.A. Pud, N.A. Ogurtsov, YuV. Noskov, S.D. Mikhaylov, YuP. Piryatinski, V.N. Bliznyuk on the importance of interface interactions in core-shell nanocomposites of intrinsically conducting polymers, Semiconductor Physics, Quantum Electronics and Optoelectronics 22 (2019) 470–478, https://doi.org/10.15407/spqeo22.04.470.
[36] N.A. Ogurtsov, Y.V. Noskov, V.N. Bliznyuk, V.G. Ilyin, J.L. Wojkiewicz, E.A. Fedorenko, A.A. Pud, Evolution and interdependence of structure and properties of nanocomposites of multiwall carbon nanotubes with polyaniline, J. Phys. Chem. C 120 (2016) 230–242, https://doi.org/10.1021/acs.jpcc.5b08524.
[37] L. Vovchenko, L. Matzui, O. Brusylovets, V. Oliynyk, V. Launets, A. Shames, O. Yakovenko, N. Skoryk, Synthesis and properties of ferrite nanopowders for epoxy-barium hexaferrite-nanocarbon composites for microwave applications, Mater. Werkst. 47 (2016) 139–148, https://doi.org/10.1002/mawe.201600487.
[38] S. Kovar, J. Valouch, H. Urbancokova, Calculation of shielding effectiveness of materials for security devices, MATEC Web of Conferences 125 (2017), 02036, https://doi.org/10.1051/matecconf/201712502036.
[39] Shielding efficiency measuring methods and systems/saju daniel, and sabu thomas//, in: M. Jaroszewski, S. Thomas, A.V. Rane (Eds.), Advanced Materials for Electromagnetic Shielding: Fundamentals, Properties, and Applications, John Wiley & Sons, Inc., 2019, https://doi.org/10.1002/9781119128625.ch14 (Chapter 4).
[40] H. Wang, K. Zheng, X. Zhang, T. Du, C. Xiao, X. Ding, C. Bao, L. Chen, X. Tian, Segregated poly(vinylidene fluoride)/MWCNTs composites for high-performance electromagnetic interference shielding, Composites Part A 90 (2016) 606–613, https://doi.org/10.1016/j.compositesa.2016.08.030.
[41] Œuvres Completes d'Augustin Fresnel/Augustin Jean Fresnel, Published by Imprimerie imperiale in Paris, French, 1866. https://archive.org/details/uvrescompltesda00fresgoog/page/n168/mode/thumb.
[42] K. Chrissafis, D. Bikiaris, Can nanoparticles really enhance thermal stability of polymers? Part I: an overview on thermal decomposition of addition polymers, Thermochim. Acta 523 (2011) 1–24, https://doi.org/10.1016/j.tca.2011.06.010.
[43] S. Ray, R.P. Cooney, Thermal degradation of polymer and polymer composites, in: Handbook of Environmental Degradation of Materials, third ed., 2018, pp. 185–206, https://doi.org/10.1016/B978-0-323-52472-8.00009-5.
[44] S. Ray, A.J. Easteal, R.P. Cooney, N.R. Edmonds, Structure and properties of melt-processed PVDF/PMMA/polyaniline blends, Mater. Chem. Phys. 113 (2009) 829–838, https://doi.org/10.1016/j.matchemphys.2008.08.034.
[45] A.J. Lovinger, D.J. Freed, Inhomogeneous thermal degradation of poly(vinyidene fluoride) crystallized from the melt, Macromolecules 13 (1980) 989–994, https://doi.org/10.1021/ma60076a044.
[46] P. Han, J. Liao, J. Chang, L. Chang, W. Bao, Preparation and characterization of poly(3-methylthiophene)/CeY zeolite composites, RSC Adv. 5 (2015) 49343–49349, https://doi.org/10.1039/C5RA08683C.
[47] J. Gu, N. Li, L. Tian, Z. Lv, Q. Zhang, High thermal conductivity graphite nanoplatelet/UHMWPE nanocomposites, RSC Adv. 5 (2015) 36334–36339, https://doi.org/10.1039/C5RA03284A.
[48] N.A. Ogurtsov, A.V. Mamykin, O.L. Kukla, A.S. Pavluchenko, M.V. Borysenko, YuP. Piryatinski, J.-L. Wojkiewicz, A.A. Pud, The impact of interfacial interactions on structural, electronic, and sensing properties of poly(3-methylthiophene) in core-shell nanocomposites. Application for chemical warfare agent simulants detection, Macromol. Mater. Eng. 307 (2022), 2100762, https://doi.org/10.1002/mame.202100762.
[49] R. Pal, Electromagnetic, Mechanical, and Transport Properties of Composite Materials, CRC Press, Boca Raton, 2015. https://www.routledge.com/Electromagnetic-Mechanical-and-Transport-Properties-of-Composite-Materials/Pal/p/book/9781420089219.